Computational and Structural Biotechnology Journal 23 (2024) 2669–2679

Contents lists available at ScienceDirect

Computational and Structural Biotechnology Journal

journal homepage: www.elsevier.com/locate/csbj

Research article

Investigating how HIV-1 antiretrovirals differentially behave as substrates and inhibitors of P-glycoprotein via molecular dynamics simulations

Daisy I. Fuchs, Lauren D. Serio, Sahana Balaji, Kayla G. Sprenger *

Department of Chemical and Biological Engineering, University of Colorado Boulder, Boulder, CO 80303, USA

ARTICLE INFO

Keywords:
P-glycoprotein
HIV-1 antiretrovirals
Molecular dynamics simulations
Blood-brain barrier
Molecule docking
Binding energetics
Protein dynamics
Conformational changes
Efflux
Molecular mechanisms

ABSTRACT

HIV-1 can rapidly infect the brain upon initial infection, establishing latent reservoirs that induce neuronal damage and/or death, resulting in HIV-Associated Neurocognitive Disorder. Though anti-HIV-1 antiretrovirals (ARVs) suppress viral load, the blood-brain barrier limits drug access to the brain, largely because of highly expressed efflux proteins like P-glycoprotein (P-gp). While no FDA-approved P-gp inhibitor currently exists, HIV-1 protease inhibitors show promise as partial P-gp inhibitors, potentially enhancing drug delivery to the brain. Herein, we employed docking and molecular dynamics simulations to elucidate key differences in P-gp's interactions with several antiretrovirals, including protease inhibitors, with known inhibitory or substrate-like behaviors towards P-gp. Our results led us to hypothesize new mechanistic details of small-molecule efflux by and inhibition of P-gp, where the "Lower Pocket" in P-gp's transmembrane domain serves as the primary initial site for small-molecule binding. Subsequently, this pocket merges with the more traditionally studied drug binding site—the "Upper Pocket"—thus funneling small-molecule drugs, such as ARVs, towards the Upper Pocket for efflux. Furthermore, our results reinforce the understanding that both binding energetics and changes in protein dynamics are crucial in discerning small molecules as non-substrates, substrates, or inhibitors of P-gp. Our findings indicate that interactions between P-gp and inhibitory ARVs induce bridging of transmembrane domain helices, impeding P-gp conformational changes and contributing to the inhibitory behavior of these ARVs. Overall, insights gained in this study could serve to guide the design of future P-gp-targeting therapeutics for a wide range of pathological conditions and diseases, including HIV-1.

1. Introduction

HIV-1 establishes latent reservoirs throughout the body early in infection, remaining hidden and inactive inside immune cells for years [1], hindering a complete cure for HIV-1. Early treatment with HIV-1 antiretrovirals (ARVs) effectively reduces the total latent HIV-1 reservoir size [1,2] by up to 100-fold after three years [1]. However, ARVs primarily target active HIV-1 replication, relying on their ability to quickly reach sites in the body where latent reservoirs are established to stimulate resident immune cells to robust and early action [3,4]. The challenge is not all sites in the body where latent reservoirs typically form are effectively targeted by ARVs, such as the brain [5].

HIV-1 enters the brain within weeks of initial infection, primarily via transport across the blood-brain-barrier (BBB) by HIV-infected monocytes [6]. Once there, HIV-1 chiefly infects microglia, the brain's resident macrophages, establishing a latent reservoir in these cells [7]. The presence of HIV-1 in the brain often causes neurodegeneration, resulting in HIV-associated neurocognitive disorders (HAND) [8,9]. The mechanisms underlying HAND are complex and involve a combination of viral, immune, and inflammatory factors. Early ARV treatment is associated with a reduced risk of HAND, further stressing the need for rapid and robust targeting of ARVs to the brain [5].

In contrast to the apparent ease with which HIV-1 enters the brain, it is very challenging for most therapeutics, including ARVs, which must passively diffuse across the complex lipid membrane of the BBB [10] and then avoid clearance by highly-expressed efflux proteins like P-glycoprotein (P-gp) [11]. The BBB is regarded as one of the most difficult barriers to permeate in the human body, preventing 98% of all small molecules from crossing [12]. Thus, the efficacy of ARVs in preventing HAND and HIV-1 reservoir formation is limited by their poor BBB transport abilities.

Major gaps persist in our understanding of how drugs interact with BBB efflux proteins, evidenced by the lack of an FDA-approved inhibitor for P-gp, one of the most widely studied efflux proteins [13]. P-gp

* Corresponding author.
E-mail address: kayla.sprenger@colorado.edu (K.G. Sprenger).

https://doi.org/10.1016/j.csbj.2024.06.025
Received 15 April 2024; Received in revised form 18 June 2024; Accepted 18 June 2024
Available online 21 June 2024

utilizes ATP hydrolysis to transition between inward- and outward-facing configurations (Fig. 1). In the inward-facing configuration, the two nucleotide binding domain (NBD) regions on either "arm" of P-gp, where ATP binds, are spaced apart, allowing substrates to bind in the transmembrane domain (TMD). Ligand binding and ATP hydrolysis bring the NBD regions together, altering the TMD's conformation and creating a pore for substrates to be effluxed back out into the blood stream, rather than to penetrate the brain [14].

A prior *in silico* study utilizing mouse P-gp revealed that this configurational change is differentially impacted by substrate and inhibitor binding, emphasizing the importance of understanding these interactions for effective drug development [15]. Another *in silico* study performed molecular docking with a structure of human P-gp [16], shedding light on these substrate binding pockets, previously delineated by Shapiro and Ling [17]. Additionally, Ferreira et al. uncovered a third binding site in the lower region of the TMD, which interacts with P-gp modulators. The authors suggested that known P-gp modulators primarily interact with this lower pocket, potentially facilitating bridging between the two halves of the TMD. Importantly, however, molecular dynamics (MD) simulations were not conducted on the docked complexes to refine the locations of these pockets and comprehend their dynamics in the context of ligand binding and P-gp conformational changes [18].

Upregulation of P-gp in tissues like the BBB and tumors can lead to drug resistance, preventing therapeutic drug concentrations from being achieved [19]. While complete P-gp inhibition is a potential solution, it raises the risk of allowing toxins into critical tissues, including the brain and placenta [13,14]. Therefore, drug candidates for P-gp inhibition must navigate the task of modulating P-gp dynamics without compromising essential protective functions.

HIV-1 protease inhibitors (PIs) are a class of ARVs shown to behave as partial P-gp inhibitors [20–22]. PIs were first designed in 1995 to block intravirion protein degradation, preventing HIV-1 virion maturation [23]. As early as 1999, scientists noted that the PI ritonavir had

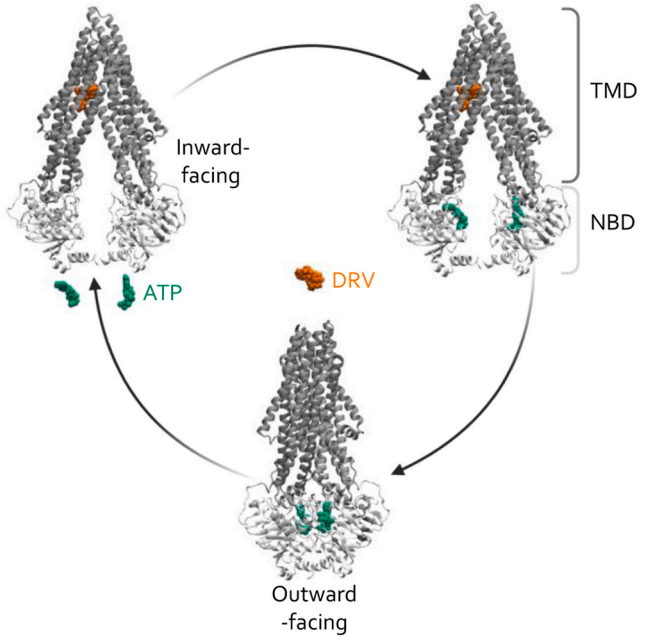

Fig. 1. Simplified overview of the efflux cycle of P-gp. Largescale structural changes in P-gp from the inward- to the outward-facing configuration are driven by the hydrolysis of ATP (shown in green) upon small-molecule binding to the transmembrane domain (TMD; dark gray). Following binding, the nucleotide binding domains (NBD regions; light gray) come together, closing the TMD to create a pore for substrates, such as DRV (shown in orange), to pass back into the blood. The NBD regions are on the cytosolic side of the membrane.

P-gp inhibition properties and could boost the bioavailability of other HIV-1 drugs [24]. PIs exhibit structural and chemical similarities as a result of their optimization to inhibit the active site of HIV-1 protease. However, not all PIs act as P-gp inhibitors, and those that do vary in their inhibitory capacities [25,26]. This underscores the need for a deeper understanding of P-gp/PI interactions, encompassing PIs that exhibit substrate and/or inhibitor behaviors. Such insights can pave the way for the development of P-gp inhibitors that play the delicate role of inhibiting without causing generalized cell toxicity.

The underlying mechanisms of P-gp inhibition, along with the dual role of PIs as both substrates and inhibitors of P-gp, remain to be fully explored. Determining the molecular-level interactions between PIs and P-gp can be achieved using *in silico* tools, such as MD. Yet, only a small handful of *in silico* studies have been conducted to date to investigate the interactions between HIV-1 PIs and P-gp [27–30]. The majority of these studies utilized the structure of non-human P-gp (i.e., P-gp from Mus musculus) [28–30], as the structure of human P-gp was not experimentally resolved until 2018. One of these studies, albeit utilizing the structure of human P-gp [27], focused solely on the outward-facing structure (PDB: 6C0V [31]) and was limited to examining the interactions between just two PIs with P-gp. Thus, there remains a need for more extensive *in silico* studies to understand the mechanistic impacts of PIs on the dynamics of human P-gp.

We employed MD to investigate the interactions of four HIV-1 PIs—darunavir (DRV), ritonavir (RTV), saquinavir (SQV), and nelfinavir (NFV)—with P-gp. We utilized the structure of P-gp in its inward-facing configuration, in which most BBB-diffusing drugs will likely first encounter P-gp *in vivo*. While RTV, NFV, and SQV have documented P-gp inhibitory effects, they can also be effluxed [20–22]. DRV has been shown to be a P-gp substrate, with no evidence of inhibition [32–34]. We also included Zidovudine (AZT) in our study, a well-established HIV-1 nucleoside analog reverse transcriptase inhibitor, to serve as a control for pure substrate-like behavior towards P-gp [33,35–37]. The new insights gained through this study into small-molecule binding energetics and protein dynamics paint a more in-depth picture of the P-gp efflux mechanism and how it can be perturbed by the presence of inhibitors, knowledge that may inform the design of future P-gp-targeting therapeutics.

2. Methods

2.1. Small-molecule parameterization

The initial structures of SQV, NFV, RTV, DRV, and AZT were isolated from published, experimentally resolved structures [38–42]. Subsequently, these structures underwent optimization and parameterization through Hartree-Fock calculations performed in Gaussian, utilizing the 6–31 G(d)/6–31 G(d) basis set [43]. Antechamber [44] was employed to assign electrostatic point charges through restrained electrostatic potential (RESP [45]) charge fitting. The formatted simulation input files for GROMACS were generated using tLEaP [46] and ACPYPE [47]. For Lennard-Jones parameters, force constants, and equilibrium constants in the PI input files, we referred to the Amber-99SBILDN force field [48]. In the case of ATP, a similar parameterization process using Gaussian and Antechamber was applied. However, a charge of -4 was assigned to the structure with two fewer hydrogens, and this structure was then combined with Mg^{2+} to model ATP in its bioactive form, which was used for all docking calculations and MD simulations with ATP [49,50].

2.2. Molecular docking with AutoDock Vina

The structure of human P-gp used in this study, which was not membrane bound, consistent with other recent P-gp studies [34,51], was obtained from the AlphaFold model (AF-P08183-F1) [52,53]. We validated this structure against other published, experimentally resolved structures of human P-gp [54,55], which contained substantial missing

residues and thus were not utilized. High structural alignment was observed between the AlphaFold and experimentally resolved structures in Visual Molecular Dynamics (VMD) (Fig. S1). To prevent potential interference with small-molecule docking, the unstructured terminal regions (residues 1–32 and residues 634–690) were removed due to their tendency to adopt physically irrelevant conformations during simulations. Before the docking phase, the resulting P-gp structure underwent equilibration and a 300 ns production simulation, following the methods described in the ensuing section. Blind docking, using AutoDock Vina, [56–58] was conducted on both the energy-minimized P-gp structure and an MD-equilibrated P-gp structure extracted after 250 ns of production simulation. Each structure was partitioned into 22 grids, measuring 30 Å x 30 Å x 30 Å, aligned to ensure consistent positioning for both P-gp structures. The grids were strategically arranged to promote overlap, ensuring comprehensive consideration of the full spatial range of each P-gp structure during blind docking. The selection of models for subsequent MD simulations was based on biological relevance, such as their location in the known drug binding pocket, and consistently high estimated affinity within a given grid. The top nine conformations in each grid were output, resulting in a total of 198 docking poses for each P-gp/small molecule combination.

2.3. Molecular dynamics simulations

The GROMACS 2021 MD engine [59] was employed for all simulations in this study, and the box size for all simulations was approximately 15 nm × 15 nm × 15 nm. Water and ions were modeled using the TIP3P [60] and Amber99SB-ILDN [48] force fields, respectively. The simulation protocol involved energy minimization, followed by a 1 ns NVT simulation using the Bussi-Donadio-Parrinello thermostat [61] to maintain a temperature of 310 K. Subsequently, a 1 ns NPT simulation was conducted with the same thermostat and the Berendsen barostat [62] to sustain a system pressure of 1 bar. Finally, production simulations were carried out on each system using the same thermostat and the Parrinello-Rahman barostat [63] at 310 K and 1 bar. As a control, a production simulatoin of 300 ns was performed of P-gp in solution. Systems of equilibrated P-gp in complex with ARVs underwent an additional 150 ns production simulation, during which all systems converged. The LINCS algorithm was utilized to constrain bonds between hydrogen and heavy atoms [64]. All simulations employed full periodic boundary conditions and particle mesh Ewald [65] summation with a cutoff of 1.2 nm for calculating long-range electrostatic forces. Non-bonded interactions were computed over a 1.2 nm range and shifted to prevent artifacts from energy discontinuities. Neighbor lists were updated every 10 steps, using a cutoff of 1.4 nm.

2.4. Simulation trajectory analysis

The convergence of each system was assessed through root-mean-square deviation (RMSD) all-to-all calculations [66] (Fig. S2), and the recovery of bulk water density far from the protein was confirmed by computing the radial distribution function of water (Fig. S3). To capture the dynamics of P-gp during the simulation, we computed the distance between the center of mass of each NBD. For evaluating the free energy of binding between small molecules and P-gp, the GROMACS plugin, *g_mmpbsa*, was employed, applying the Molecular Mechanics Poisson-Boltzmann Surface Area (MM/PBSA) approach over the last 50 ns of each production simulation [67,68]. Contact residues, representing P-gp residues within 4 Å of the small molecule, were determined using VMD to delineate the binding pocket and track its evolution throughout the entire production simulation [69].

3. Results and discussion

3.1. Anti-HIV-1 ARVs are distinguishable as substrates or inhibitors of P-gp based on average docking affinities, supported by binding free energy calculations from MD simulations

We conducted comprehensive docking of the five ARVs across the full structure of P-gp using AutoDock Vina (see Methods for gridding procedures). This analysis encompassed both the initial, energy-minimized configuration of P-gp (Fig. 2A, top) and the converged structure obtained after 250 ns of production MD simulation (Fig. 2A, bottom). Based on docking outputs, we identified biologically-relevant binding sites with consistently high docking-estimated affinities across all grids, leading to the discovery of three conserved sites for ARV binding.

The first site, referred to as the "Upper Pocket," is situated within the TMD, spanning grids 3–5 in the initial P-gp configuration and grid 4 in the converged configuration (Fig. 2B, dark green highlighted regions). We note that the Upper Pocket corresponds to what is referred to as the M-site in other published literature [18]. Particularly evident in the converged P-gp configuration, spikes in docking affinity toward more negative (favorable) values were observed for all five ARVs at this site. This finding provides validation of our approach, as the Upper Pocket is the known drug binding pocket for P-gp efflux. Visual inspection of the docked complexes revealed that the Upper Pocket's more conserved nature in the converged P-gp structure—spanning just a single grid instead of three in the initial configuration—arises from heightened geometric constraints in the TMD. Calculations of the solvent accessible surface area (SASA) supported this observation, demonstrating reduced accessibility of the Upper Pocket in the converged P-gp structure (Fig. S4).

The second site, referred to as the "Lower Pocket," is also situated within the TMD, directly below the Upper Pocket, and is similar to the R and H sites indicated by Ferreira et al [18]. The Lower Pocket spans grids 8–9 in the initial P-gp configuration and grid 9 in the converged configuration (Fig. 2B, dark blue highlighted regions). Similar to the Upper Pocket, we observed a sharp increase in docking affinity for each of the five ARVs at this site, particularly evident in the converged configuration. Again, akin to the Upper Pocket, the Lower Pocket appears more conserved in the converged versus initial configuration due to a reduced SASA for ligand binding. Illustrated in more detail in a later section, the Lower and Upper Pockets associate together as the NBDs close and the structures converge. Uniquely, this behavior has not been observed in past *in silico* P-gp studies that did not perform MD simulations on the binding pockets after small-molecule docking to elucidate these intricate dynamics [18].

Finally, the third site is that of the previously-defined NBD, a known binding site of ATP [14] (Fig. 2B, light green highlighted regions). The NBD binding site singularly spans grid 18 in both the initial and converged P-gp configurations, showing characteristic spikes in affinity for all ARVs. Later, we discuss observed similarities and differences in how ATP itself binds to the NBD versus the ARVs. One other location of interest in the NBD that emerged was grid 13, which is highly conserved across all ARVs in the converged P-gp configuration. However, this site appears unremarkable in the initial P-gp configuration, exhibiting a lower average ARV affinity than the other identified binding sites. As our primary focus with regards to the NBD was on interactions with ATP, further exploration of this site in the context of ARVs was not pursued.

The rank order of binding affinities estimated from docking was determined for each ARV in each grid and averaged across all 22 grids (Fig. 2C). This average rank order effectively differentiated between the ARVs based on their known classifications as pure substrates (DRV and AZT) or partial inhibitors (SQV, NFV, and RTV) of P-gp. This differentiation was observed, to varying degrees, for both the initial (Fig. 2C, top) and converged structure (Fig. 2C, bottom) of P-gp. However, the use of the initial structure resulted in more statistically significant

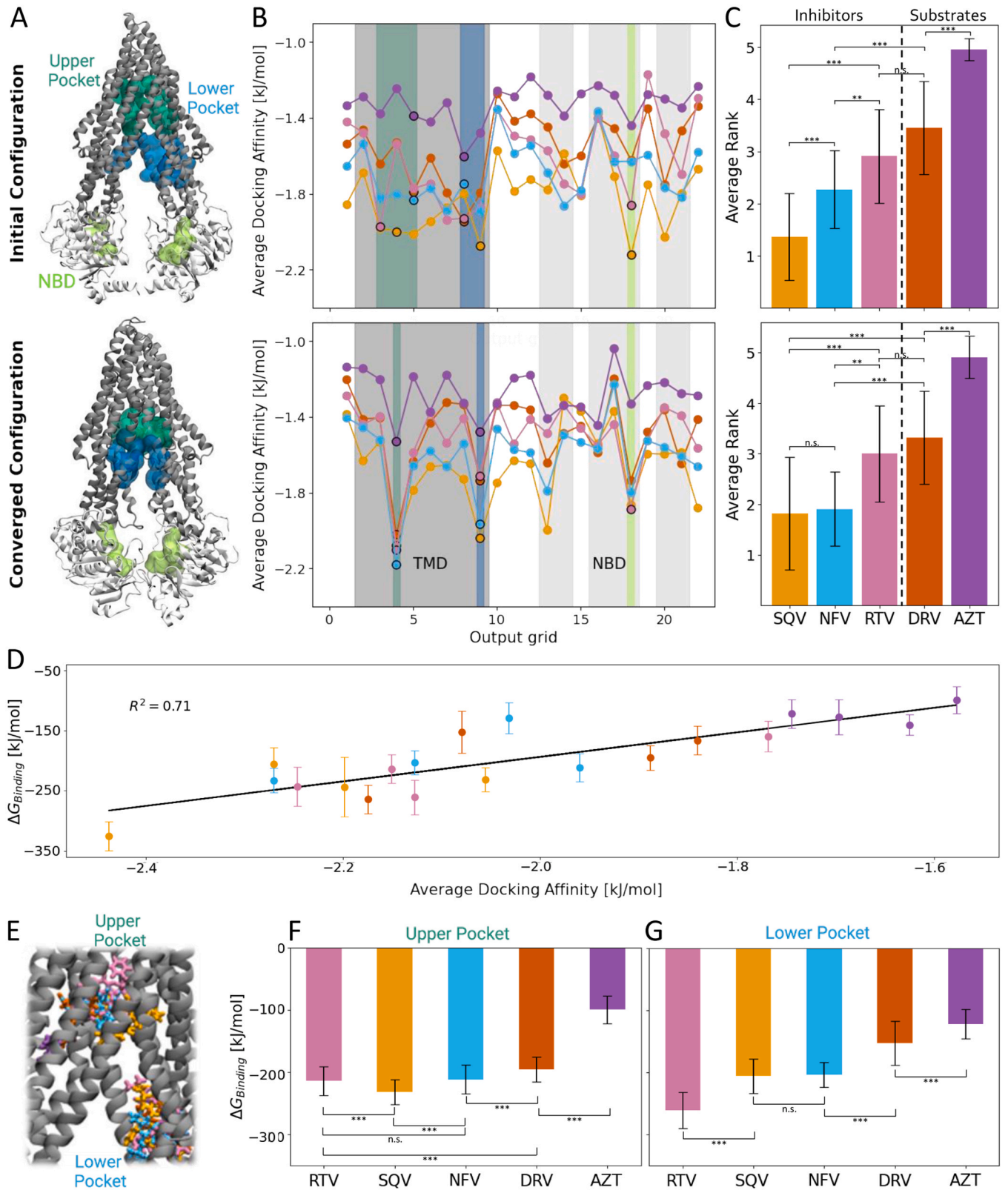

Fig. 2. ARV substrates and inhibitors of P-gp are distinguishable by binding affinity. (A-C) Data shown for the initial (top) and converged (bottom) P-gp starting configurations. (A) P-gp binding domains identified via docking and MD: Upper Pocket (dark green), Lower Pocket (dark blue), and NBD regions (light green). (B) ARV binding affinities estimated from AutoDock Vina, averaged for each gridded location on P-gp. MD-simulated locations are circled in black; identified binding domains are shown in the same colors as in (A). (C) ARV affinity rank orders averaged across all 22 grids from (B). A dotted line distinguishes ARVs with known inhibitory and substrate-like behavior towards P-gp. (D) Binding affinities calculated from docking vs. MD, using the MM/PBSA approach. (E) Snapshot of ARVs bound in the Upper and Lower Pockets of the initial P-gp configuration. (F-G) Comparison of binding free energies from MD (MM/PBSA approach) for ARVs bound in the (F) Upper Pocket and (G) Lower Pocket. Statistical significance in (C), (F), and (G) was assessed with an independent two sample t-test where * ** indicates a p-value (P) < 0.0001 and * * a $P < 0.01$; else, samples are not statistically significant (n.s.).

differences among the five ARVs, despite the standard deviation for a given ARV remaining similar across the two P-gp structures. This observation aligns with the notion that the open (initial) P-gp configuration is the one in which small molecules are expected to first encounter P-gp *in vivo*, necessitating a greater ability to discriminate among small molecules. Conversely, once P-gp undergoes largescale structural changes to the closed (converged) state, small molecules are likely to be effluxed out of the brain, requiring less discriminatory capacity. Notably, the same rank orders as the averages can be obtained by analyzing ARV binding to many individual P-gp grids/binding sites, including the Lower Pocket and NBD. This implies that small molecules that bind stronger to *any* site on P-gp are, in general, more likely to bind stronger to *key* sites on P-gp that facilitate inhibition.

To validate and expand upon our initial docking observations, MD simulations were conducted on selected P-gp/ARV complexes. Each ARV was simulated bound to both the Upper and Lower Pockets of P-gp in both its initial and converged configurations, resulting in four simulations per ARV in the TMD region. The corresponding grids are depicted as black-circled points in Fig. 2B. Following the production simulations, the GROMACS tool *g_mmpbsa* was employed to implement the MM/PBSA approach for calculating the binding free energy of the complexes, averaged across the last 50 ns of the simulations (see Methods). An aggregate plot of these binding free energies from MD versus the docking affinity estimates shows a strong linear correlation (R^2 =0.71; Fig. 2D). This provides further validation of our approach and supports the notion that docking may serve as an effective initial screening tool to identify candidate P-gp inhibitors.

To gain thermodynamic insights into the mechanisms underlying P-gp inhibition, we compared the MD binding free energies of the ARVs bound to the Upper and Lower Pockets of the initial P-gp structure (Fig. 2E). No significant differences in ARV binding to these sites in the converged structure were observed. Aligning with our docking results, we noted stronger (more negative) average binding free energies for ARVs with known inhibitory behavior compared to those with known substrate-like behavior towards P-gp, both for the Upper (Fig. 2F) and Lower Pockets (Fig. 2G) in the initial structure. However, the Lower Pocket exhibited a greater discriminatory ability among ARV substrates and inhibitors based on binding free energy compared to the Upper Pocket. These variations in binding free energy suggest that substrates may unbind from the Lower Pocket more readily to efflux out of the cell after the Lower and Upper Pockets merge, while drugs with inhibitory capabilities could more effectively block other substrates from entering the TMD. The critical role of the Upper Pocket as P-gp's drug binding site, alongside its seemingly limited discriminatory capacity, suggests that, besides thermodynamics, impacts of ARV binding on P-gp *dynamics* may also be crucial for classifying them as substrates or inhibitors of P-gp. In the subsequent section, we explore the implications of ARV binding on P-gp dynamics in greater detail.

3.2. *P-gp's 'Lower Pocket' emerges as the primary initial site for small-molecule binding, while insights into inhibitor behavior are gleaned from binding to P-gp's 'Upper Pocket'*

P-gp was initially simulated in solution without ARVs to elucidate its dynamic behavior and establish a baseline for comparison with simulations where ARVs were present. Commencing from the inward-facing configuration of P-gp, the simulations revealed a gradual approach of the NBD regions towards one another over 200 ns, ultimately stabilizing at a specific distance (Fig. 3A). To measure this distance, we assessed the separation between the centers-of-mass of NBD residues 374 to 632 and 1018 to 1279. Notably, the converged distance observed in the simulation exceeded that of the experimentally resolved structure of P-gp in the outward-facing configuration by nearly 1.5 nm. This indicates ATP hydrolysis is necessary to fully "close" P-gp's structure for the transition between inward- and outward-facing configurations during efflux [70]. Fig. 3A shows that the distance between NBD regions is inversely related to the RMSD of P-gp, denoting that the primary shift in P-gp's structure during the simulations arose from NBD closure. Consequently, this association influenced the accessibility of TMD binding sites. Specifically, the Upper and Lower Pockets were observed to be spatially distinct in the initial P-gp configuration (Fig. 2A, top), while in the converged configuration, the pockets were much closer together (Fig. 2A, bottom).

To evaluate the influence of ARV binding on P-gp dynamics, we analyzed the residues within the Lower (Fig. 3B, top) and Upper Pockets (Fig. 3B, bottom) of P-gp that interacted with each ARV for at least 80% of the simulation. All ARVs were found to contact a greater number of residues in the Upper Pocket, likely due to its narrower and more confined geometry. Moreover, there was some overlap in the residues contacted by ARVs in both pockets, providing further evidence of their increased proximity as the NBD regions converged during the simulations. In the Upper Pocket, SQV and RTV were uniquely observed to contact residues around position 200 and between positions 860–950 (Fig. 3B, top, gray regions). However, the absence of contacts between the third inhibitor—NFV—and these same residues casts doubt regarding the criticality of these positions in distinguishing P-gp substrates and inhibitors. In contrast, in the Lower Pocket, all three inhibitors frequently interacted with residues around position 1000 (Fig. 3B, bottom, gray region), which were not contacted by either substrate. This supports our earlier finding that the Lower Pocket may possess a greater ability to distinguish between substrates, non-substrates, and inhibitors based on affinity and the contacts mediating it. Importantly, the observed interactions near position 1000 appear to create a bridge-like connection among TMD helices (Fig. 3D), which could impede P-gp's transition from the inward- to outward-facing configuration during efflux. To our knowledge, this bridging behavior in the Lower Pocket has not been noted in prior work, such as that by Ferreira et al., where cross-TMD interactions were only observed in the Upper Pocket [18]. Our study also found bridging in the Upper Pocket, although these interactions were considered more of a direct consequence of the smaller site's geometry.

The differential behavior observed in the Lower Pocket between pure substrates and partial inhibitors of P-gp is primarily attributed to differences in hydrophobicity among the small molecules. It is well-documented that P-gp substrates tend to be hydrophobic, and recent reviews suggest that increased hydrophobicity of a compound may enhance its ability to inhibit P-gp [14]. The three ARVs—NFV, RTV, and SQV—known as partial inhibitors of P-gp, all engage in bridging interactions across the TMD and exhibit markedly higher logP values, indicating greater hydrophobicity, compared to AZT and DRV (Table S1) [71]. To further validate this, we confirmed that verapamil, a known P-gp inhibitor that is not an ARV, has a similar logP value to the inhibitory ARVs [14]. Additionally, the inhibitory behavior of verapamil refutes the idea that AZT's pure substrate behavior is solely due to its smaller size, as both drugs have similar molecular weights and surface areas. Crucially, three out of the four amino acids found to interact with the inhibitory ARVs in the Lower Pocket are hydrophobic, underscoring the importance of strong hydrophobic interactions for P-gp inhibition.

Considering the Lower Pocket's greater discriminatory capacity alongside our earlier observation that the Lower Pocket and Upper Pocket spatially associate during NBD closure, we propose the following mechanism (Fig. 4): small molecules, upon diffusing past the NBD regions into the TMD, first encounter and bind in the Lower Pocket, where they are classified as substrates or non-substrates of P-gp based on their binding affinity. Low-affinity binders (non-substrates) have a higher probability of unbinding and exiting the Lower Pocket into the brain before the NBD regions can associate and subsequent efflux steps can occur (timescale, t; $t_{unbind} < t_{NBD\ closure}$). Conversely, intermediate-affinity binders (substrates) and high-affinity binders (inhibitors) have a higher probability of remaining bound long enough for the NBD regions to come together ($t_{unbind} > t_{NBD\ closure}$). As this occurs, the Upper and Lower Pockets spatially associate, funneling the intermediate/high-affinity binder closer to the Upper Pocket—supported through visual

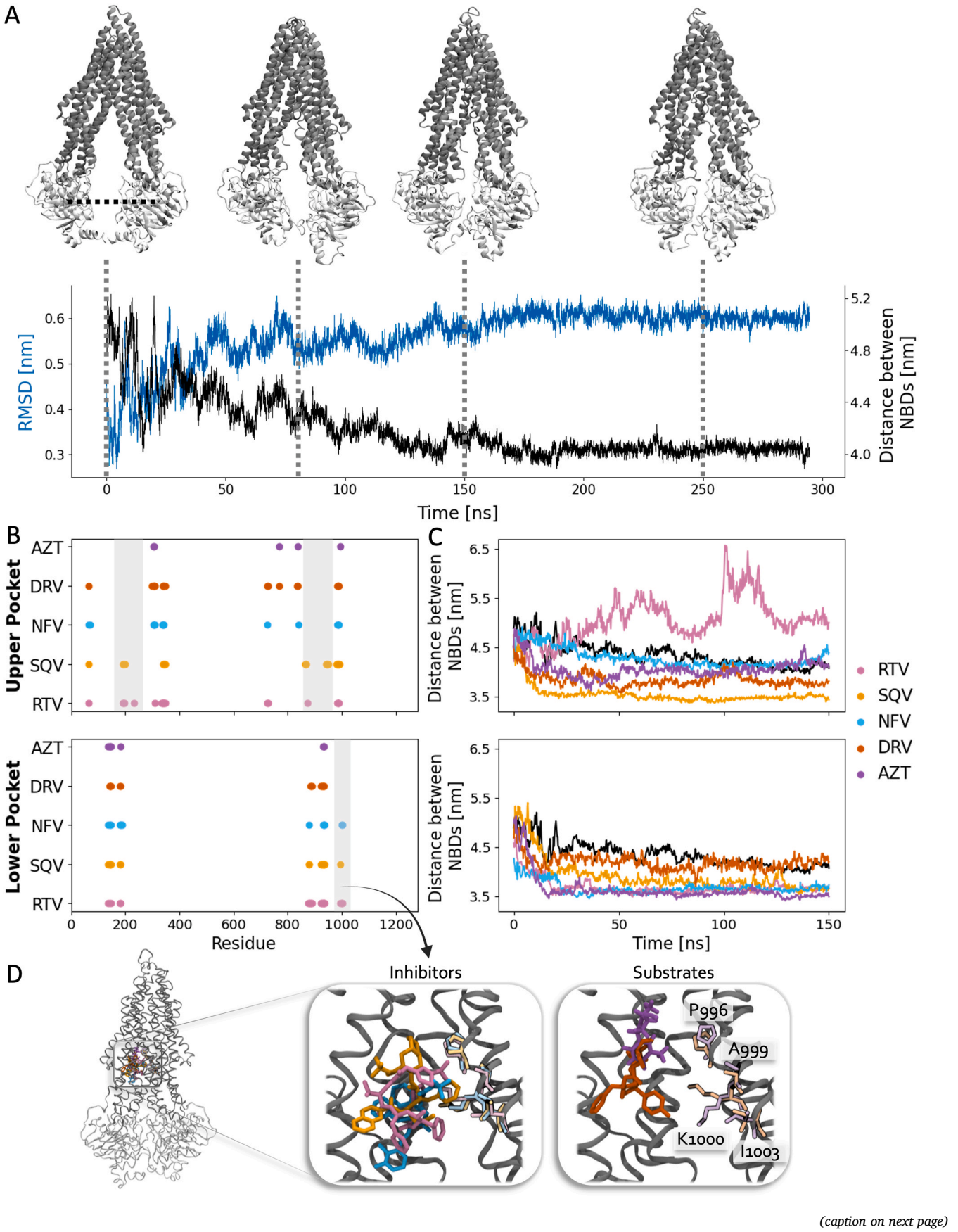

(caption on next page)

Fig. 3. Inhibitory ARVs uniquely interact with P-gp TMD helices during MD simulations. (A) Dynamics of P-gp in solution, characterized by the distance between the centers-of-mass of the two NBD regions (black line) and the root-mean-square deviation (RMSD) of P-gp's Cα atoms (blue line). Simulation snapshots are shown at the indicated timepoints of 0, 70, 150, and 250 ns, with a dotted black line visually depicting the measured distance between NBD regions. (B) Dynamics of P-gp-ARV interactions, characterized as P-gp residues in contact with (within 4 Å of) the ARV, bound to the Upper (top) and Lower (bottom) Pockets of P-gp, for at least 80% of the simulation. Gray regions highlight key differences in P-gp binding between ARV inhibitors and substrates. (C) Distance between NBD regions in the presence of ARVs bound to the Upper (top) and Lower (bottom) Pockets of P-gp, compared to P-gp alone in solution (black line). (D) Simulation snapshots highlighting differential interactions of ARV inhibitors (left) and substrates (right) with P-gp residues near position 1000. ARVs and corresponding P-gp residues from a given simulation are shown in darker and lighter shades of the same color, respectively.

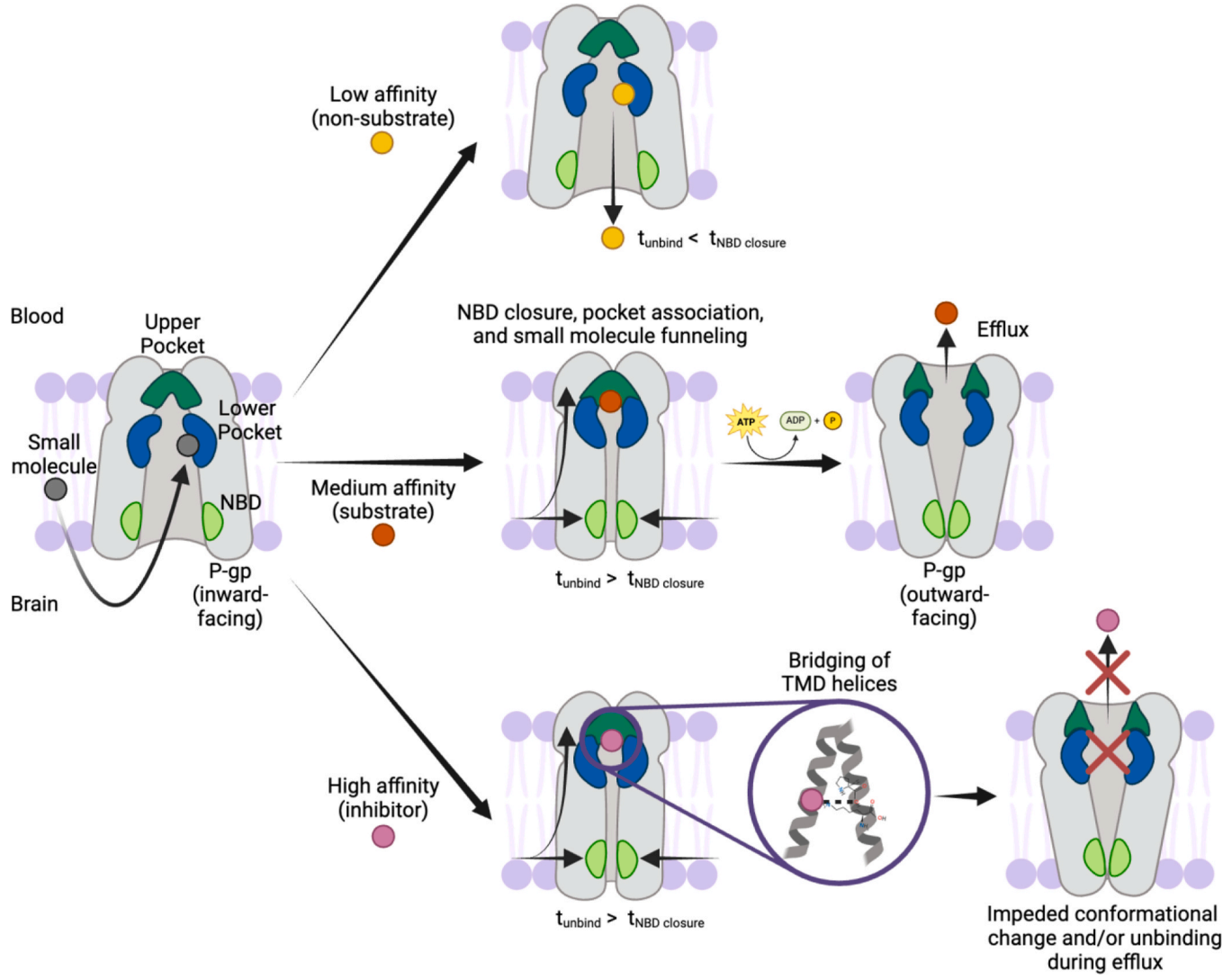

Fig. 4. Proposed mechanism for P-gp discrimination of non-substrates and substrates, and inhibition. Upon diffusing past the NBD regions into the TMD, small molecules initially bind in the Lower Pocket of P-gp, where they are classified as substrates or non-substrates based on affinity. Low-affinity binders (non-substrates) are more likely to unbind and exit into the brain before the NBD regions associate and efflux can occur (timescale, t; $t_{unbind} < t_{NBD\ closure}$). On the other hand, intermediate-affinity binders (substrates) and high-affinity binders (inhibitors) are more likely to remain bound until the NBD regions come together ($t_{unbind} > t_{NBD\ closure}$). This leads to spatial association of the Upper and Lower Pockets, positioning intermediate/high-affinity binders closer to the Upper Pocket in anticipation of efflux. Following P-gp's structural change from the inward- to outward-facing configuration, substrates are expelled. Inhibitors, due to their high affinity, may delay unbinding, hindering efflux, and/or interact uniquely with P-gp residues, potentially obstructing further P-gp configurational changes through bridge-like interactions with TMD helices.

analysis of our simulations in VMD—in preparation for efflux out of the cell. Upon P-gp's ensuing structural change from the inward- to outward-facing configuration, substrates will then unbind and be expelled from the cell. On the other hand, due to their high affinity, inhibitors may remain bound or significantly delay unbinding, thereby hindering efflux, or form unique interactions with P-gp residues that impede key configurational changes, as discussed above.

Finally, to further confirm this mechanism, we examined the effects of ARVs on the dynamics of NBD closure. The presence of all five ARVs in the Lower Pocket (Fig. 3C, bottom) prompted swift closure of the NBD regions to a similar or greater extent than with P-gp alone in solution (Fig. 3A), with little variation in dynamics observed between substrates and inhibitors. This lends credence to our proposed mechanism, suggesting that both inhibitors and substrates elicit similar responses from P-gp during the initial stages of efflux, namely NBD closure, association of the Lower and Upper pockets, and funneling of small molecules

towards the Upper Pocket. Conversely, altered and, in some cases, unstable dynamics were observed when inhibitors were bound directly to the initial configuration of P-gp in the Upper Pocket (Fig. 3C, top). Although we expect it is unlikely that the majority of small molecules bind directly to the Upper Pocket of P-gp in its initial configuration, this probability may differ between substrates and inhibitors, a line of inquiry we did not explore in detail in this study. As such, the dynamics illustrated in Fig. 3C may still yield insights into the underlying inhibition mechanisms of the studied ARVs. In particular, NFV was observed to slow NBD closure, RTV fully inhibited NBD closure, and SQV led to excessive NBD closure. Slowed NBD closure may allow substrates to unbind before the NBD regions can associate, fully-inhibited NBD closure may hinder funneling of the inhibitor to the Upper Pocket, thereby blocking substrate binding to the Lower Pocket, and excessive NBD closure may hinder ATP hydrolysis.

While previous literature has predominantly focused on the Upper Pocket, our proposed mechanism, informed by rigorous *in silico* analysis of P-gp thermodynamics and dynamics in the presence of ARVs, suggests the pivotal role of the Lower Pocket as the primary site for initial small-molecule binding and discrimination. This hypothesis is reinforced by the likelihood that small molecules, as they traverse the lipid membrane of the BBB, must fully penetrate into the intracellular space, where P-gp

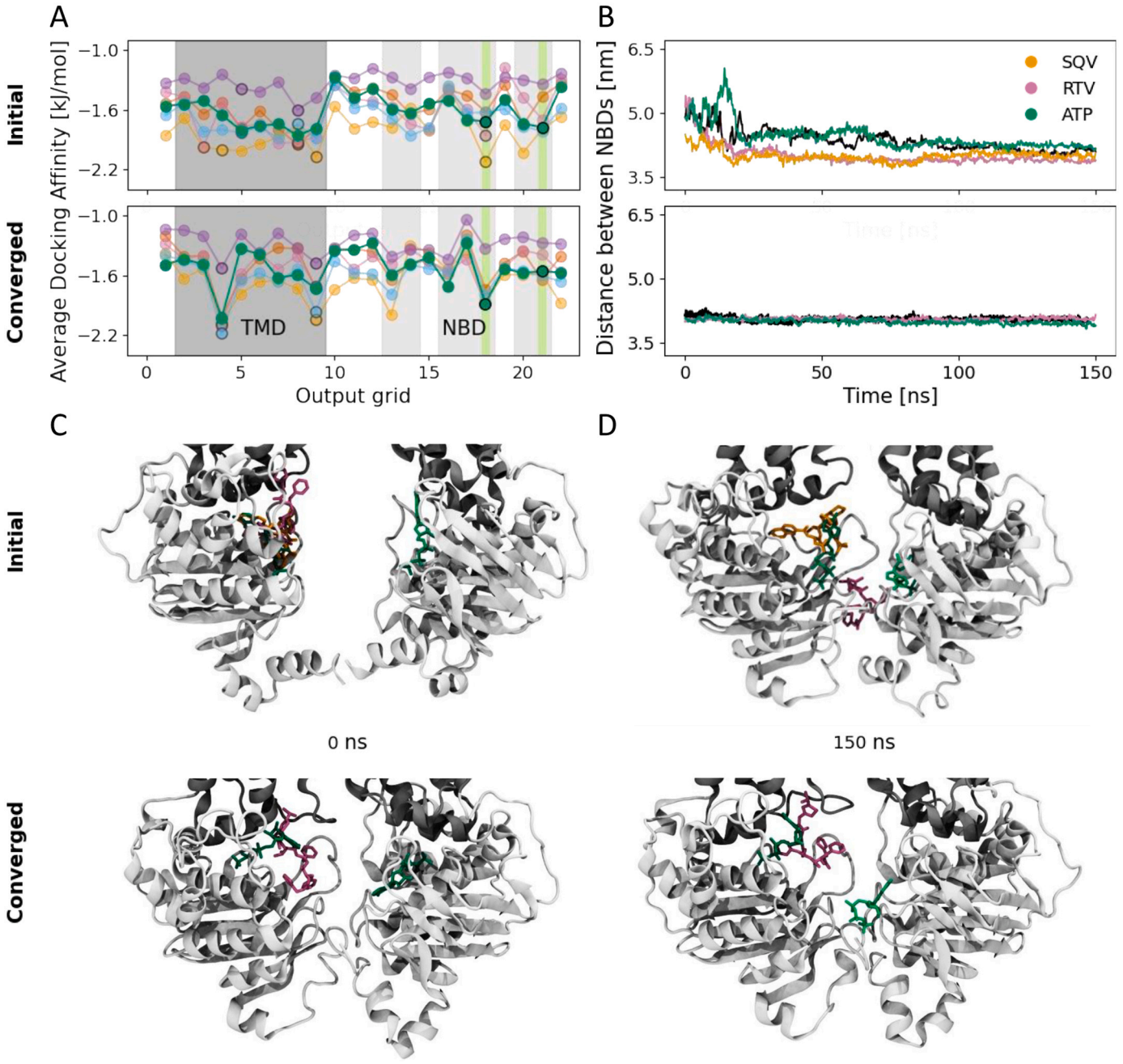

Fig. 5. Beyond ATP, inhibitory ARVs demonstrate a modest propensity to bind to the NBD. (A-D) Data shown for the initial (top) and converged (bottom) P-gp starting configurations. (A) ATP binding affinities estimated from AutoDock Vina, averaged for each gridded location on P-gp and overlaid on the ARV docking affinities presented in Fig. 2B. MD-simulated locations are circled in black; identified binding domains are shown in the same colors as in Fig. 2A-B. (B) Distance between NBD regions in the presence of bound ATP or ARVs, compared to P-gp alone in solution (black line). (C-D) Simulation snapshots highlighting ATP and ARVs bound to the NBD at 0 ns (C) and 150 ns (D). Note that each small molecule was simulated in complex with P-gp without other small molecules present, but their structures are overlaid here for simplicity on a representative protein structure. Overlaid final P-gp configurations with SQV, RTV, and ATP are shown in Fig. S8.

is more accessible, to interact meaningfully with P-gp. Consequently, they would first pass between the NBD regions and then encounter the Lower Pocket before reaching the Upper Pocket. Our proposed mechanism emphasizes the importance of further investigation into the Lower Pocket's role in discerning between substrates and inhibitors during efflux, thus influencing their fate. This underscores the Lower Pocket's potential as a crucial therapeutic target for the development of effective P-gp inhibitors.

3.3. Binding of ARV inhibitors to P-gp's NBD induces excessive NBD closure, possibly disrupting ATP binding, though interactions with the TMD remain the most likely cause for inhibition

In addition to ARVs, we explored the interactions of P-gp with ATP through molecular docking and MD simulations. We focused solely on ATP in its bioactive form in complex with Mg^{2+}, resulting in a net charge of -2, omitting the investigation of intermediary states of ATP and ADP. Upon docking the ATP complex in the NBD, we compared the contact residues between ATP and P-gp to those identified in an experimentally resolved structure of outward-facing P-gp in complex with ATP [31]. We confirmed that ATP was located in the same pockets of the NBD, with overlapping contacts. In our study ATP was treated as a control, neither a substrate nor an inhibitor, due to its established interactions with P-gp [70]. Consistent with this perspective, our docking calculations revealed that ATP exhibited intermediate binding affinity across the majority of P-gp grids (see Methods) compared to the ARVs. This observation held true for both the initial (Fig. 5A, top) and converged (Fig. 5A, bottom) P-gp configurations. Moreover, by calculating the mean rank of ATP across all grids for each P-gp configuration, we observed that the values fell squarely between those of the ARV substrates and inhibitors (Fig. 2C). This suggests that ATP defies classification as either (Fig. S5).

Notably, however, ATP exhibited heightened affinity compared to the ARVs for grids 18 and 21, particularly evident in the converged P-gp configuration (Fig. 5A, bottom). These grids correspond to the NBD region located on each "arm" of P-gp, the known ATP binding sites, lending credibility to our approach. Affinity for both sides of the NBD is biologically significant as ATP must bind to each of the two NBD regions for eventual hydrolysis to take place (Fig. 1). Interestingly, although not indicated to behave as a substrate, ATP also exhibited relatively high affinity for the Upper Pocket of the converged P-gp configuration, albeit weaker than four of the five ARVs.

As previously mentioned, ATP was not the only molecule predicted to bind to the NBD through docking simulations. Specifically, both SQV and RTV demonstrated stronger docking-predicted binding affinities than ATP to the NBD region corresponding to grid 18 in the initial P-gp configuration (Fig. 5A, top). This observation suggests that SQV and RTV could potentially act as competitive inhibitors by outcompeting or effectively displacing ATP from the binding site. To further explore these findings, we performed MD simulations of SQV and RTV bound to this NBD region (grid 18) in the initial P-gp configuration, as well as of RTV bound to the same site in the converged P-gp configuration as a control. Additionally, we performed MD with ATP bound to both NBD regions (grids 18 and 21) in both the initial and converged P-gp configurations, along with a simulation of ATP bound in the Upper Pocket of the initial P-gp configuration. As expected, when ATP was bound to both NBD regions, the dynamics of P-gp closely resembled those of P-gp alone in solution (Fig. 5B; top=initial, bottom=converged configuration), indicating the importance of ATP hydrolysis occurring through intermediate molecules like ADP in mediating additional P-gp configurational changes. Interestingly, when ATP was bound to the Upper Pocket of the initial P-gp configuration, the dynamics initially exhibited instability before converging to the same NBD distance observed with P-gp alone in solution (Fig. S6). The simulation also required a longer time to converge than the majority of the complexes with ARVs. These findings provide additional evidence that ATP likely does not function as a canonical substrate of P-gp.

Conversely, the presence of RTV and SQV in the NBD of the initial P-gp configuration resulted in excessive NBD closure (Fig. 5B, top), leading to a smaller distance between the NBD regions compared to ATP-bound P-gp or P-gp alone in solution. Notably, RTV did not alter P-gp's dynamics when bound to the NBD of the converged configuration (Fig. 5B, bottom). This behavior of ARVs in the NBD of the initial P-gp configuration echoes our earlier findings with SQV bound to the Upper Pocket of this same structure and may provide further insights into the inhibition mechanisms of these ARVs. Importantly, however, our earlier docking analysis revealed that the affinities of SQV and RTV for this NBD site are comparable to or weaker than their affinities for the Upper and Lower Pockets of P-gp (Fig. 2B). This trend was reinforced by post-MD MM/PBSA calculations (Fig. S7), emphasizing the weaker binding of SQV and RTV to the NBD site. Furthermore, we observed that when RTV was bound to the NBD in the initial P-gp configuration, it eventually dissociated and diffused away from the NBD during the simulation (Fig. 5C-D). Collectively, these results support our conclusion that while SQV and RTV exhibit some inhibitory tendencies towards the NBD, they likely preferentially interact with and impact the dynamics of P-gp's TMD.

4. Conclusions and future outlook

Herein, we employed an *in silico* approach to investigate the dual behavior of anti-HIV-1 antiretroviral (ARV) drugs as both substrates and inhibitors of P-glycoprotein (P-gp). Our investigation led to the proposal of a novel inhibition mechanism, highlighting the crucial role of the Lower Pocket binding site in the transmembrane domain (TMD) of P-gp. We hypothesize that non-substrates, lacking sufficient affinity for P-gp, unbind and return to the cytosol before efflux can occur. In contrast, substrates and inhibitors bind with an intermediate to high affinity in the TMD of P-gp, initially in the Lower Pocket. Subsequently, P-gp undergoes a configurational change that leads substrates and inhibitors to be funneled towards the Upper Pocket—the canonical drug binding site of P-gp. [14] Substrates exhibit weaker binding affinity to P-gp compared to inhibitors, resulting in their efflux out of the cell. Meanwhile, inhibitors demonstrate strong binding affinity for P-gp, delaying their unbinding and efflux. Furthermore, inhibitors may even form bridge-like interactions between TMD helices on both sides of the Lower Pocket, further preventing efflux. Notably, this proposed mechanism is reliant upon both binding energetics and protein dynamics, contributing to its complexity.

The results of our study support our proposed mechanism. Molecular docking with AutoDock Vina revealed both the Upper and Lower Pockets as probable binding sites for all five ARVs studied, regardless of their role as substrates or inhibitors, across two different P-gp starting structures, referred to as the 'initial' and 'converged' configurations of P-gp. The former closely resembled the experimentally resolved structure of P-gp, while the latter represented the output, equilibrated structure from a molecular dynamics (MD) simulation. While binding affinities estimated from docking could discriminate between the known ARV substrates and inhibitors, confirmatory results with increased statistical significance were obtained using rigorous free-energy calculations from MD simulations. In particular, inhibitory ARVs exhibited markedly higher binding affinities than substrate-like ARVs for the Lower Pocket of P-gp compared to the Upper Pocket, further emphasizing the role of the Lower Pocket as the primary initial binding site for small-molecule, affinity-based discrimination by P-gp.

We suggest that the previous lack of understanding regarding the Lower Pocket and its involvement in P-gp efflux and inhibition can be attributed to the absence of small-molecule binding at this site in the few existing experimentally resolved human P-gp structures. This absence likely stems from the proposed intermediary nature of binding to the Lower Pocket within P-gp's overall efflux mechanism. In the future, initial binding of small molecules to the Lower Pocket could potentially be verified by first employing a drug that specifically binds to the

nucleotide binding domain (NBD) regions of P-gp and inhibits their closure. Alternatively, engineering P-gp itself to remain in the open, inward-facing configuration could facilitate the observation of Lower Pocket binding. Subsequent crystallization with a known P-gp substrate, such as Darunavir (DRV) or Atazanavir (AZT), used in this study, could reveal binding to the Lower Pocket.

In addition to energetics, the binding of ARVs in the Lower Pocket influenced the dynamic configurational changes observed in P-gp during the simulation. These dynamics, characterized by the distance between NBD regions, differed greatly in the presence of ARVs from those of P-gp in solution, which indicated a convergence towards a "closed" state. Through analysis of ARV-P-gp contact residues, inhibitors were distinguished by their binding in the Lower Pocket, where they exhibited interactions bridging across the TMD, as mentioned above. We posit that these interactions may impede subsequent structural changes of P-gp from the inward- to the outward-facing configuration. However, further studies on P-gp's largescale conformational changes during efflux are warranted to confirm this hypothesis. If confirmed, our results could pave the way for the design of new P-gp inhibitors that leverage these TMD bridging interactions to impede substrate efflux, particularly across the blood-brain barrier (BBB).

The behaviors of ARV inhibitors bound to the NBD were also investigated alongside bioactive ATP, which served as a control. Post-simulation free energy calculations revealed that the ARV inhibitors exhibited weaker affinity for the NBD compared to the TMD. This suggests that while there may be some potential for competitive inhibition in the NBD, ARVs are more likely to inhibit P-gp efflux through interactions in the TMD.

Finally, while this study has provided valuable insights into the inhibition mechanism of P-gp by ARVs, additional research is warranted on ARV transport in the presence of membrane-bound P-gp. We anticipate that such studies will further underscore the significance of the Lower Pocket in initial small-molecule binding by shedding light on the binding preferences of the small molecules as they diffuse through P-gp's intracellular cavity. Further studies on the kinetics of P-gp binding and unbinding events should also be conducted, as our study focused solely on the thermodynamics of binding and therefore did not fully account for all random protein motions or fluctuations that could impact both the affinity and stability of small molecule-P-gp interactions. Furthermore, alongside additional *in silico* investigations, there is a pressing need for relevant *in vitro* studies that directly compare the P-gp inhibition potential of various small molecules. Anti-HIV-1 protease inhibitors, such as ritonavir (RTV), utilized in this study, have shown promise as P-gp inhibitors without life-threatening side effects, [24] highlighting their potential for use in expanded pharmaceutical applications or as a baseline for improved inhibitor design.

Author statement

The submitted work has not been published previously. The submitted work is not under consideration for publication elsewhere. The publication is approved by all authors and the responsible authorities where the work was carried out. If accepted, the submitted work will not be published elsewhere in the same form, in English or in any other language, including electronically without the written consent of the copyright-holder. The Author declares no conflict of interest. The Author declares that generative artificial intelligence (AI) and AI-assisted technologies were not used in the writing process.

CRediT authorship contribution statement

Sahana Balaji: Investigation. **Kayla Sprenger:** Writing – review & editing, Writing – original draft, Visualization, Validation, Supervision, Software, Resources, Project administration, Methodology, Investigation, Funding acquisition, Formal analysis, Data curation, Conceptualization. **Daisy Fuchs:** Writing – review & editing, Writing – original draft, Visualization, Validation, Methodology, Investigation, Funding acquisition, Formal analysis, Data curation, Conceptualization. **Lauren Serio:** Writing – review & editing, Methodology, Investigation, Formal analysis.

Declaration of Competing Interest

The authors declare that they have no known competing financial interests or personal relationships that could have appeared to influence the work reported in this paper.

Acknowledgements

This work utilized resources from the University of Colorado Boulder Research Computing Group, which is supported by the National Science Foundation (awards ACI-1532235 and ACI-1532236), the University of Colorado Boulder, and Colorado State University. Research reported in this publication was also supported by the National Institute of Mental Health and National Institute of Neurological Disorders and Stroke under Award Number R21MH132159.

Appendix A. Supporting information

Supplementary data associated with this article can be found in the online version at doi:10.1016/j.csbj.2024.06.025.

References

[1] Ananworanich J, et al. HIV DNA set point is rapidly established in acute hiv infection and dramatically reduced by early ART. EBioMedicine 2016;11:68–72.
[2] Ananworanich J, Dubé K, Chomont N, Jackson HM. How does the timing of antiretroviral therapy initiation in acute infection affect HIV reservoirs? Curr Opin HIV AIDS 2015;10:18–28.
[3] Buzon MJ, et al. Long-term antiretroviral treatment initiated at primary HIV-1 infection affects the size, composition, and decay kinetics of the reservoir of HIV-1-Infected CD4 T Cells. J Virol 2014;88:10056–65.
[4] Laanani M, et al. Impact of the timing of initiation of antiretroviral therapy during primary HIV-1 INfection on the Decay of Cell-associated HIV-DNA. Clin Infect Dis 2015;60:1715–21.
[5] Ash MK, Al-Harthi L, Schneider JR. HIV in the brain: Identifying viral reservoirs and addressing the challenges of an HIV cure (Preprint at) Vaccines 2021;vol. 9. https://doi.org/10.3390/vaccines9080867.
[6] Ash MK, Al-Harthi L, Schneider JR. HIV in the brain: identifying viral reservoirs and addressing the challenges of an HIV cure. Vaccin (Basel) 2021;9:867.
[7] Wallet C, et al. Microglial Cells: the main HIV-1 reservoir in the brain. Front Cell Infect Microbiol 2019;9:362.
[8] Li W, Galey D, Mattson MP, Nath A. Molecular and cellular mechanisms of neuronal cell death in HIV dementia. Neurotox Res 2005 8:1 2005;8:119–34.
[9] Clifford DB. HIV-associated neurocognitive disorder (Preprint at) Curr Opin Infect Dis 2017;vol. 30:117–22. https://doi.org/10.1097/QCO.0000000000000328.
[10] Osborne O, Peyravian N, Nair M, Daunert S, Toborek M. The paradox of HIV blood–brain barrier penetrance and antiretroviral drug delivery deficiencies. Trends Neurosci 2020;43:695–708.
[11] Park S, Sinko PJ. P-glycoprotein and mutlidrug resistance-associated proteins limit the brain uptake of saquinavir in mice. J Pharmacol Exp Ther 2005;312:1249–56.
[12] Choudhari M, et al. Evolving new-age strategies to transport therapeutics across the blood-brain-barrier. Int J Pharm 2021;599:120351.
[13] Lai JI, Tseng YJ, Chen MH, Huang CYF, Chang PMH. Clinical perspective of FDA approved drugs with P-glycoprotein inhibition activities for potential cancer therapeutics. Front Oncol 2020;10:561936.
[14] Ahmed Juvale II, Abdul Hamid AA, Abd Halim KB, Che Has AT. P-glycoprotein: new insights into structure, physiological function, regulation and alterations in disease. Heliyon 2022;8:e09777.
[15] Xing J, Huang S, Heng Y, Mei H, Pan X. Computational Insights into allosteric conformational modulation of P-Glycoprotein by substrate and inhibitor binding. 2020, Vol. 25, Page 6006 Molecules 2020;25:6006.
[16] Ferreira RJ, Ferreira MJU, Dos Santos DJVA. Insights on P-glycoproteins efflux mechanism obtained by molecular dynamics simulations. J Chem Theory Comput 2012;8:1853–64.
[17] Shapiro AB, Ling V. Positively cooperative sites for drug transport by P-glycoprotein with distinct drug specificities. Eur J Biochem 1997;250:130–7.
[18] Ferreira RJ, Ferreira U, V A dos Santos DJ. Molecular docking characterizes substrate-binding sites and efflux modulation mechanisms within P-Glycoprotein. J Chem Inf Model 2013;53:29.
[19] Fromm MF. Importance of P-glycoprotein at blood-tissue barriers (Preprint at) Trends Pharmacol Sci 2004;vol. 25:423–9. https://doi.org/10.1016/j.tips.2004.06.002.

[20] Martinec O, et al. Anti-HIV and anti-hepatitis C virus drugs inhibit P-glycoprotein efflux activity in Caco-2 cells and precision-cut rat and human intestinal slices. Antimicrob Agents Chemother 2019;63.

[21] Marzolini C, Paus E, Buclin T, Kim RB. Polymorphisms in human MDR1 (P-glycoprotein): recent advances and clinical relevance. Clin Pharm Ther 2004;75:13–33.

[22] Herédi-Szabó, K. *et al.* A P-gp vesicular transport inhibition assay-Optimization and validation for drug-drug interaction testing. (2013) doi:10.1016/j.ejps.2013.04.032.

[23] Lv Z, Chu Y, Wang Y. HIV protease inhibitors: a review of molecular selectivity and toxicity. HIV/AIDS - Res Palliat Care 2015;7:95–104.

[24] Drewe J. ürgen *et al.* HIV protease inhibitor ritonavir: a more potent inhibitor of P-glycoprotein than the cyclosporine analog SDZ PSC 833. Biochem Pharm 1999;57:1147–52.

[25] Storch CH, Theile D, Lindenmaier H, Haefeli WE, Weiss J. Comparison of the inhibitory activity of anti-HIV drugs on P-glycoprotein. Biochem Pharm 2007;73:1573–81.

[26] Fujimoto H, et al. P-Glycoprotein mediates efflux transport of darunavir in human intestinal Caco-2 and ABCB1 gene-transfected renal LLC-PK1 cell lines HHS public access. Biol Pharm Bull 2009;vol. 32.

[27] Kehinde, I., Ramharack, P., Nlooto, M. & Gordon, M. Molecular dynamic mechanism(s) of inhibition of bioactive antiviral phytochemical compounds targeting cytochrome P450 3A4 and P-glycoprotein. https://doi.org/10.1080/07391102.2020.1821780 **40**, 1037–1047 (2020).

[28] Swedrowska M, et al. In silico and in vitro screening for p-glycoprotein interaction with tenofovir, darunavir, and dapivirine: an antiretroviral drug combination for topical prevention of colorectal HIV transmission. Mol Pharm 2017;14:2660–9.

[29] Gualdesi MS, Briñón MC, Quevedo MA. Intestinal permeability of lamivudine (3TC) and two novel 3TC prodrugs. Experimental and theoretical analyses. Eur J Pharm Sci 2012;47:965–78.

[30] Quevedo MA, Nieto LE, Briñón MC. P-glycoprotein limits the absorption of the anti-HIV drug zidovudine through rat intestinal segments. Eur J Pharm Sci 2011;43:151–9.

[31] Kim Y, Chen J. Molecular structure of human P-glycoprotein in the ATP-bound, outward-facing conformation. Science (1979) 2018;359:915–9.

[32] Rehman, S. *et al.* Role of P-Glycoprotein Inhibitors in the Bioavailability Enhancement of Solid Dispersion of Darunavir. (2017) doi:10.1155/2017/8274927.

[33] Kim JY, Park YJ, Lee BM, Yoon S. Co-treatment With HIV protease inhibitor nelfinavir greatly increases late-phase apoptosis of drug-resistant KBV20C cancer cells independently of P-glycoprotein inhibition. Anticancer Res 2019;39:3757–65.

[34] Swedrowska M, et al. In silico and in vitro screening for P-glycoprotein interaction with tenofovir, darunavir, and dapivirine: an antiretroviral drug combination for topical prevention of colorectal HIV transmission. Mol Pharm 2017;14:2660–9.

[35] Chapy H, et al. Blood–brain and retinal barriers show dissimilar ABC transporter impacts and concealed effect of P-glycoprotein on a novel verapamil influx carrier. Br J Pharm 2016;173:497.

[36] Wang F, et al. Acute liver failure enhances oral plasma exposure of zidovudine in rats by downregulation of hepatic UGT2B7 and intestinal P-gp. Acta Pharm Sin 2017;38:1554.

[37] Quevedo MA, Nieto LE, Briñón MC. P-glycoprotein limits the absorption of the anti-HIV drug zidovudine through rat intestinal segments. Eur J Pharm Sci 2011;43:151–9.

[38] Liu Z, et al. Insights into the mechanism of drug resistance: X-ray structure analysis of multi-drug resistant HIV-1 protease ritonavir complex. Biochem Biophys Res Commun 2013;431:232–8.

[39] Tie Y, et al. Atomic resolution crystal structures of HIV-1 protease and mutants V82A and I84V with saquinavir. Protein: Struct, Funct Genet 2007;67:232–42.

[40] Kožíšek M, et al. Molecular analysis of the HIV-1 resistance development: enzymatic activities, crystal structures, and thermodynamics of nelfinavir-resistant HIV protease mutants. J Mol Biol 2007;374:1005–16.

[41] Wang Y, et al. The higher barrier of darunavir and tipranavir resistance for HIV-1 protease. Biochem Biophys Res Commun 2011;412:737–42.

[42] Zhu L, Yang F, Chen L, Meehan EJ, Huang M. A new drug binding subsite on human serum albumin and drug–drug interaction studied by X-ray crystallography. J Struct Biol 2008;162:40–9.

[43] Frisch MJ, et al. Gaussian 09, Revision B.01 (Preprint at). Gaussian 09, Revision B.01. *Wallingford CT*: Gaussian, Inc.,; 2009.

[44] Wang J, Wang W, Kollman PA, Case DA. Automatic atom type and bond type perception in molecular mechanical calculations. J Mol Graph Model 2006;25:247–60.

[45] Cornell WD, Cieplak P, Christopher, /, Bayly I, Kollman PA. Application of RESP charges to calculate conformational energies, hydrogen bond energies, and free energies of solvation. J Am Chem Soc 1993;115:9620–31.

[46] Case DA, et al. The amber biomolecular simulation programs. J Comput Chem 2005;26:1668–88.

[47] Sousa Da Silva AW, Vranken WF. ACPYPE - AnteChamber PYthon Parser interfacE. BMC Res Notes 2012;5:1–8.

[48] Lindorff-Larsen K, et al. Improved side-chain torsion potentials for the Amber ff99SB protein force field. Protein: Struct, Funct Bioinforma 2010;78:1950–8.

[49] Buelens FP, Leonov H, De Groot BL, Grubmüller H. ATP-Magnesium coordination: protein structure-based force field evaluation and corrections. J Chem Theory Comput 2021;17:1922–30.

[50] Meagher KL, Redman LT, Carlson HA. Development of polyphosphate parameters for use with the AMBER force field. J Comput Chem 2003;vol. 24. ⟨http://www.interscience.wiley.com/jpages/0192⟩.

[51] Kehinde I, Ramharack P, Nlooto M, Gordon M. Molecular dynamic mechanism(s) of inhibition of bioactive antiviral phytochemical compounds targeting cytochrome P450 3A4 and P-glycoprotein. J Biomol Struct Dyn 2022;40:1037–47.

[52] Jumper J, et al. Highly accurate protein structure prediction with AlphaFold. 2021 596:7873 Nature 2021;596:583–9.

[53] Varadi M, et al. AlphaFold Protein Structure Database: massively expanding the structural coverage of protein-sequence space with high-accuracy models. Nucleic Acids Res 2022;50:D439–44.

[54] Alam A, Kowal J, Broude E, Roninson I, Locher KP. Structural insight into substrate and inhibitor discrimination by human P-glycoprotein. Science (1979) 2019;363:753–6.

[55] Urgaonkar S, et al. Discovery and characterization of potent dual P-glycoprotein and CYP3A4 Inhibitors: design, synthesis, cryo-em analysis, and biological evaluations. J Med Chem 2022;65:191–216.

[56] Forli S, et al. Computational protein-ligand docking and virtual drug screening with the AutoDock suite. Nat Protoc 2016;11:905–19.

[57] Trott O, Olson AJ. AutoDock Vina: Improving the speed and accuracy of docking with a new scoring function, efficient optimization, and multithreading. *J Comput Chem* NA-NA 2009. https://doi.org/10.1002/jcc.21334.

[58] Eberhardt J, Santos-Martins D, Tillack AF, Forli S. AutoDock vina 1.2.0: new docking methods, expanded force field, and python bindings. J Chem Inf Model 2021;61:3891–8.

[59] Abraham, M.J. *et al.* GROMACS: High performance molecular simulations through multi-level parallelism from laptops to supercomputers. doi:10.1016/j.softx.2015.06.001.

[60] Neria E, Fischer S, Karplus M. Simulation of activation free energies in molecular systems. J Chem Phys 1996;105:1902–21.

[61] Bussi G, Donadio D, Parrinello M. Canonical sampling through velocity rescaling. J Chem Phys 2007;126:14101.

[62] Berendsen HJC, Postma JPM, Van Gunsteren WF, Dinola A, Haak JR. Molecular dynamics with coupling to an external bath. J Chem Phys 1984;81:3684–90.

[63] Parrinello M, Rahman A. Polymorphic transitions in single crystals: a new molecular dynamics method. J Appl Phys 1981;52:7182–90.

[64] Hess B, Bekker H, Berendsen HJC, Fraaije JGEM. LINCS: a linear constraint solver for molecular simulations. J Comput Chem 1997;vol. 18.

[65] Darden T, York D, Pedersen L. Particle mesh Ewald: An N·log(N) method for Ewald sums in large systems. J Chem Phys 1993;98:10089–92.

[66] Grossfield A, et al. Best practices for quantification of uncertainty and sampling quality in molecular simulations [Article v1.0. Living J Comput Mol Sci 2018;1.

[67] Kumari R, Kumar R, Lynn A. G-mmpbsa -A GROMACS tool for high-throughput MM-PBSA calculations. J Chem Inf Model 2014;54:1951–62.

[68] Wang C, Greene D, Xiao L, Qi R, Luo R. Recent developments and applications of the MMPBSA method (Preprint at) Front Mol Biosci 2018;vol. 4. https://doi.org/10.3389/fmolb.2017.00087.

[69] Humphrey W, Dalke A, Schulten KVMD. Visual molecular dynamics. J Mol Graph 1996;14:33–8.

[70] Dehghani-Ghahnaviyeh S, Kapoor K, Tajkhorshid E. Conformational changes in the nucleotide-binding domains of P-glycoprotein induced by ATP hydrolysis. FEBS Lett 2021;595:735–49.

[71] Kim S, et al. PubChem 2023 update. Nucleic Acids Res 2022;51.